JOURNAL OF SPACECRAFT AND ROCKETS
Vol. 55, No. 3, May–June 2018

Convex Optimization for Power Tracking of Double-Gimbal Variable-Speed Control Moment Gyroscopes

Takahiro Sasaki*
Osaka Prefecture University, Sakai 599-8531, Japan
John Alcorn† and Hanspeter Schaub‡
University of Colorado, Boulder, Colorado 80309
and
Takashi Shimomura§
Osaka Prefecture University, Sakai 599-8531, Japan

DOI: 10.2514/1.A33944

This Paper addresses an integrated power/attitude control system for a spacecraft with two double-gimbal variable-speed control moment gyroscopes. Double-gimbal variable-speed control moment gyroscopes are of interest because a single device is a three-degree-of-freedom attitude actuator. A double-gimbal variable-speed control moment gyroscope has two gimbal axes and one variable-speed wheel. A primary advantage of adopting this actuator is to reduce the number of actuators, which leads to reducing the total mass and volume allocation within the spacecraft. In this Paper, first, the dynamical equations of motion of a spacecraft equipped with multiple double-gimbal variable-speed control moment gyroscopes are developed. Then, two types of steering laws are proposed for two double-gimbal variable-speed control moment gyroscopes. These steering laws attain three-axis attitude control and power tracking by using the wheels as energy storage devices while considering both singularity avoidance and wheel spin equalization. The controller design applies multiobjective gain scheduling with linear parameter-varying control theory, which can evaluate both optimality and robustness. Finally, numerical simulation examples of the orbiting spacecraft attitude tracking problem demonstrate the effectiveness of the proposed gain-scheduling controller and two steering laws for the integrated power/attitude control system.

Nomenclature

$\mathcal{B}$	=	body-fixed frame
G_{gi}, G_{go}	=	direction matrices of inner/outer gimbal axes of double-gimbal variable-speed control moment gyroscopes
$\mathcal{G}_i$, $\mathcal{G}_o$	=	inner/outer gimbal axes frame
G_{ws}	=	direction matrix of spin axes of double-gimbal variable-speed control moment gyroscopes
$\boldsymbol{H}$	=	total angular momentum, N · m · s
$\boldsymbol{H}_B$	=	angular momentum of the spacecraft excluding double-gimbal variable-speed control moment gyroscopes, N · m · s
$\boldsymbol{H}_{gi}$, $\boldsymbol{H}_{go}$	=	angular momentum of inner/outer gimbal, N · m · s
$\boldsymbol{H}_{ws}$	=	angular momentum of wheel, N · m · s
$[I_s]$	=	inertia matrix of the spacecraft including double-gimbal variable-speed control moment gyroscopes as point of masses, kg · m^2
$[I_{gi}]$, $[I_{go}]$	=	inertia matrices of inner/outer gimbal axes, kg · m^2
$[I_{ws}]$	=	inertia matrix of wheel spin axes, kg · m^2
$[J]$	=	inertia matrix of the spacecraft including double-gimbal variable-speed control moment gyroscopes, kg · m^2
$\boldsymbol{L}$	=	total external torque, N · m
$\mathcal{N}$	=	inertial frame
n	=	number of double-gimbal variable-speed control moment gyroscopes
$\boldsymbol{P}_{\mathrm{RW}}$	=	power of reaction wheels, W
$\boldsymbol{T}_{\mathrm{RW}}$	=	kinetic energy of reaction wheels, J
$\boldsymbol{u}$	=	control torque, N · m
$\boldsymbol{u}_{\mathrm{CMG}}$	=	output torque of control moment gyroscopes, N · m
$\boldsymbol{u}_{\mathrm{RW}}$	=	output torque of reaction wheels, N · m
$\mathcal{W}$	=	spin axes frame
$\boldsymbol{\delta}_i$, $\boldsymbol{\delta}_o$	=	inner/outer gimbal angle vector, rad
$\boldsymbol{\rho}$	=	scheduling parameter vector
$\boldsymbol{\sigma}$, $\boldsymbol{\sigma}_e$	=	modified Rodrigues parameters and error modified Rodrigues parameters
$\boldsymbol{\Omega}$	=	wheel spin rate vector, rad/s
$\boldsymbol{\omega}$	=	angular velocity vector of the spacecraft, rad/s

Received 13 April 2017; revision received 18 August 2017; accepted for publication 14 February 2018; published online 27 April 2018.

*Graduate Student, Department of Aerospace Engineering, Graduate School of Engineering, Research Fellow of Japan Society for the Promotion of Science; Visiting Scholar, University of Colorado, Boulder, CO 80309. Student Member AIAA.

†Graduate Research Assistant, Department of Aerospace Engineering Science, Colorado Center for Astrodynamics Research. Student Member AIAA.

‡Alfred T. and Betty E. Look Professor of Engineering, Department of Aerospace Engineering Science, Colorado Center for Astrodynamics Research. Associate Fellow AIAA.

§Professor, Department of Aerospace Engineering, Graduate School of Engineering. Senior Member AIAA.

I. Introduction

SPACECRAFT components such as sensors, attitude actuators, and batteries are only provided within limited mass and volume allocation in the spacecraft design process. The size of the batteries or the number of attitude actuators is strictly constrained, particularly when mission-specific equipment must occupy most of the inner space of the spacecraft. Spacecraft usually have chemical batteries to store the energy generated by the solar panel. On the other hand, chemical batteries have problems such as large weight or stringent requirements such as required temperature range or resistance to cosmic radiation. As an alternative, using high-speed flywheels as dual-function devices for both attitude actuation and energy storage have been suggested [1,2]. Because many spacecraft already have flywheels for the purpose of attitude stabilization or pointing/three-axis attitude control, mass and volume within the spacecraft may be conserved by reducing the mass and volume allocation of the batteries and using the flywheels as dual-function devices. This

concept is called the integrated power/attitude control system (IPACS) [3–6].

The satellite dynamics are generally described through a set of nonlinear differential equations. Most recent studies about attitude control used nonlinear controllers such as Lyapunov function-based controllers [7,8]. With Lyapunov function-based controllers, the overall stability of attitude control is always guaranteed. However, the closed-loop control performance is not discussed in detail. To study such control performance, a linear parameter-varying (LPV) control theory [9–12] is applied to the attitude control problems [13,14]. Using the LPV control theory, the spacecraft dynamics are modeled as an LPV system to avoid difficulties arising from nonlinearities in the dynamics. A gain-scheduled (GS) controller is applied to this model using linear matrix inequalities (LMIs). To solve LMIs simultaneously, a multiobjective GS controller for evaluating both optimality and robustness can be easily designed [15,16].

There are a variety of types of momentum exchange devices (MEDs) that have flywheels. The primary benefit of using such MEDs is their availability for long-term operation without using any fuel as thrusters do. MEDs include reaction wheels (RWs) and control moment gyroscopes (CMGs). RWs are often used for spacecraft attitude control [17,18]. Because RWs cannot provide large torques, CMGs are often used for missions that demand high-speed attitude maneuvering abilities. Single-gimbal CMGs (SGCMGs) are the most common type of CMG devices. Here, the rotor is only able to gimbal about a single body-fixed axis to produce the desired control torque [19–21]. Single-gimbal variable-speed CMGs are a hybrid system that has two functions of a RW and an SGCMG. The extra degree of freedom in the wheel spin rate enables avoiding the classical SGCMG singularities at the cost of additional power and large rotor speed changes [22–25]. On the other hand, a double-gimbal VSCMG (DGVSCMG) has two gimbals and a variable-speed wheel. A DGVSCMG can generate three-dimensional torques. This advantage enables three-axis attitude control with one DGVSCMG [26–28]. However, a wheel mechanical failure is serious for a DGVSCMG device. Once its wheel has failed, a DGVSCMG is unable to generate torque. Once its gimbals have failed, high-speed attitude maneuver cannot be attained because the torque from the variable-speed wheel is much smaller than any other torques produced by gimbaling. To avoid such situations, it is convenient to introduce redundancy. In this context, there are few studies in which the dynamics and steering laws are provided for two parallel DGVSCMGs that have two parallel outer gimbal axes fixed to the spacecraft body. Cui and He [29] discussed the singularity avoidance steering law with a mode switching method based on singularity measurement. Sasaki and Shimomura [30] showed the fault-tolerant operating method for two parallel DGVSCMGs while switching between a two-Double-gimbal CMG (DGCMG) mode and a one-DGVSCMG mode.

The IPACS of a spacecraft with multiple RWs has been studied previously [3]. Moreover, some research [4–6] adapts the IPACS to spacecraft with multiple Variable-speed CMG (VSCMGs). However, there has been no previous study to consider the IPACS of a spacecraft with DGVSCMGs. This Paper considers the problem of a spacecraft with two parallel DGVSCMGs. First, the dynamical equation of motion (EOM) of a spacecraft equipped with multiple DGVSCMGs is developed. Based on the developed dynamics, an LPV model of a spacecraft with two parallel DGVSCMGs is obtained and the GS controller under mixed $\mathcal{H}_2/\mathcal{H}_\infty$ constraints is designed to guarantee optimality and robustness at the same time. Next, two types of steering laws for the IPACS are proposed while considering both singularity avoidance and wheel spin equalization. Finally, numerical simulation examples of the orbiting spacecraft attitude tracking problem demonstrate the effectiveness of the proposed GS controller and two steering laws for the IPACS.

II. Equation of Motion

The spacecraft considered in this Paper is assumed to be a rigid body and contains multiple DGVSCMG devices as modeled in Fig. 1. The body-fixed frame $\mathcal{B}$ is represented by a set of unit vectors: $\hat{\boldsymbol{x}}_B$, $\hat{\boldsymbol{y}}_B$, and $\hat{\boldsymbol{z}}_B$. The inertial frame is given by $\mathcal{N}$. The symbols $\mathcal{G}_o$, $\mathcal{G}_i$,

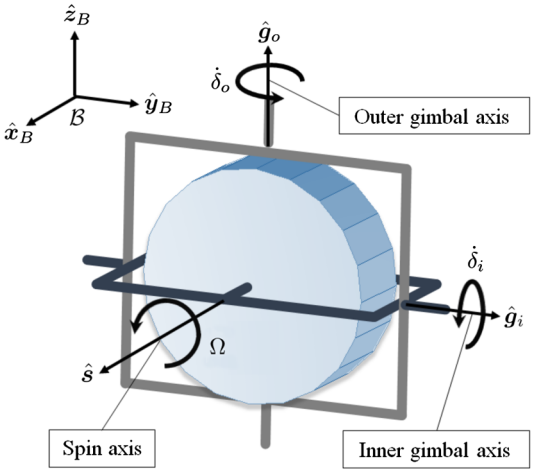

Fig. 1 DGVSCMG frames and axes illustration.

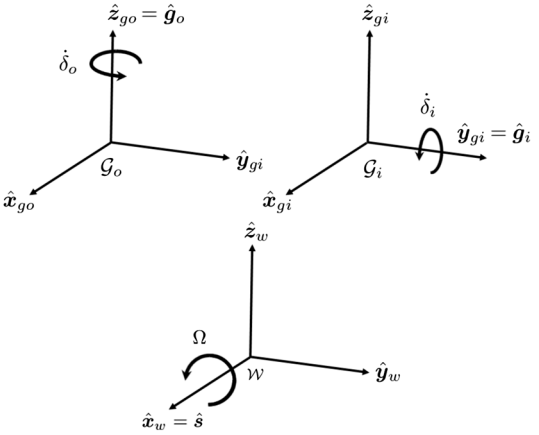

Fig. 2 Definition of DGVSCMG's frame.

and $\mathcal{W}$ denote the outer gimbal axis frame, the inner gimbal axis frame, and the wheel spin axis frame, respectively. The basis vectors of $\mathcal{G}_o$, $\mathcal{G}_i$, and $\mathcal{W}$ are defined as in Fig. 2. Note that the outer gimbal frame $\mathcal{G}_o$ is oriented such that the $\hat{\boldsymbol{z}}_{go}$ is aligned with the outer gimbal rotation axis $\hat{\boldsymbol{g}}_o$, the inner gimbal frame $\mathcal{G}_i$ is oriented such that the $\hat{\boldsymbol{y}}_{gi}$ is aligned with the inner gimbal rotation axis $\hat{\boldsymbol{g}}_i$, and the vector $\hat{\boldsymbol{x}}_w$ in the wheel spin frame $\mathcal{W}$ is the same direction toward the wheel spin axis $\hat{\boldsymbol{s}}$. Assuming that the flywheel is symmetric about the inner gimbal rotation axis $\hat{\boldsymbol{g}}_i$, the inner gimbal frame and the wheel spin frame coincide with each other as $\mathcal{G}_i = \mathcal{W}$. The inertia matrices at each frame are introduced. Because $\mathcal{G}_o$ frame unit axes are aligned with the principal outer gimbal frame axes, the jth outer gimbal inertia matrix $[I_{goj}]$ is expressed in the $\mathcal{G}_o$ frame components as the constant diagonal matrix:

$$ {}^{\mathcal{G}_o}[I_{goj}] = {}^{\mathcal{G}_o}\begin{bmatrix} I_{goj,x} & 0 & 0 \\ 0 & I_{goj,y} & 0 \\ 0 & 0 & I_{goj,z} \end{bmatrix} \tag{1} $$

Assuming that the flywheel is symmetric about the inner gimbal rotation axis, because ${}^{\mathcal{W}}[I_{wsj}] = {}^{\mathcal{G}_i}[I_{wsj}]$, the jth inner gimbal frame and wheel spin frame inertia matrices are expressed as

$$ {}^{\mathcal{G}_i}[I_{gij}] = {}^{\mathcal{G}_i}\begin{bmatrix} I_{gij,x} & 0 & 0 \\ 0 & I_{gij,y} & 0 \\ 0 & 0 & I_{gij,z} \end{bmatrix}, \quad {}^{\mathcal{G}_i}[I_{wsj}] = {}^{\mathcal{G}_i}\begin{bmatrix} I_{wsj,x} & 0 & 0 \\ 0 & I_{wsj,y} & 0 \\ 0 & 0 & I_{wsj,z} \end{bmatrix} \tag{2} $$

where $I_{wsj,y} = I_{wsj,z}$. Let the direction cosine matrix (DCM) $[\mathcal{A}_1\mathcal{A}_2]$ transform vectors written in the $\mathcal{A}_2$ frame into the vectors expressed in the $\mathcal{A}_1$ frame. Using the DCM $[\mathcal{B}\mathcal{G}_o]$ and $[\mathcal{G}_o\mathcal{G}_i]$, the constant

diagonal inertia matrices ${}^{\mathcal{G}_o}[I_{goj}]$, ${}^{\mathcal{G}_i}[I_{gij}]$, and ${}^{\mathcal{G}_i}[I_{wsj}]$ are expressed with components taken in the $\mathcal{B}$ frame as the time-varying matrices as follows:

$$ {}^{\mathcal{B}}[I_{goj}] = [\mathcal{BG}_o]^{\mathcal{G}_o}[I_{goj}][\mathcal{BG}_o]^T \tag{3a} $$

$$ {}^{\mathcal{B}}[I_{gij}] = [\mathcal{BG}_o][\mathcal{G}_o\mathcal{G}_i]^{\mathcal{G}_i}[I_{gij}][\mathcal{G}_o\mathcal{G}_i]^T[\mathcal{BG}_o]^T \tag{3b} $$

$$ {}^{\mathcal{B}}[I_{wsj}] = [\mathcal{BG}_o][\mathcal{G}_o\mathcal{G}_i]^{\mathcal{G}_i}[I_{wsj}][\mathcal{G}_o\mathcal{G}_i]^T[\mathcal{BG}_o]^T \tag{3c} $$

Here, the EOM of a spacecraft with n DGVSCMGs is considered to be expanded on the EOM of a spacecraft with a single DGVSCMG [26]. The total inertial angular momentum $\boldsymbol{H}$ is described by

$$ \boldsymbol{H} = \boldsymbol{H}_B + \boldsymbol{H}_{go} + \boldsymbol{H}_{gi} + \boldsymbol{H}_{ws} \tag{4} $$

with

$$ \boldsymbol{H}_B = [I_s]\boldsymbol{\omega}_{\mathcal{B}/\mathcal{N}} \tag{5a} $$

$$ \boldsymbol{H}_{go} = [I_{go}]\sum_{j=1}^{n}\boldsymbol{\omega}_{\mathcal{G}_{oj}/\mathcal{N}} \tag{5b} $$

$$ \boldsymbol{H}_{gi} = [I_{gi}]\sum_{j=1}^{n}\boldsymbol{\omega}_{\mathcal{G}_{ij}/\mathcal{N}} \tag{5c} $$

$$ \boldsymbol{H}_{ws} = [I_{ws}]\sum_{j=1}^{n}\boldsymbol{\omega}_{\mathcal{W}_j/\mathcal{N}} \tag{5d} $$

where

$$ \omega_{\mathcal{G}_{oj}/\mathcal{N}} = \omega_{\mathcal{B}/\mathcal{N}} + \dot{\delta}_{oj}\hat{\boldsymbol{g}}_{oj} \tag{6a} $$

$$ \omega_{\mathcal{G}_{ij}/\mathcal{N}} = \boldsymbol{\omega}_{\mathcal{B}/\mathcal{N}} + \dot{\delta}_{oj}\hat{\boldsymbol{g}}_{oj} + \dot{\delta}_{ij}\hat{\boldsymbol{g}}_{ij} \tag{6b} $$

$$ \omega_{\mathcal{W}_j/\mathcal{N}} = \omega_{\mathcal{B}/\mathcal{N}} + \dot{\delta}_{oj}\hat{\boldsymbol{g}}_{oj} + \dot{\delta}_{ij}\hat{\boldsymbol{g}}_{ij} + \Omega\hat{\boldsymbol{s}}_j \tag{6c} $$

The inertia tensors of all DGVSCMGs are assumed to be identical, and $[I_s]$ is the inertia matrix of a spacecraft (including the DGVSCMGs as point masses) about the overall spacecraft center of mass. Note that ${}^{\mathcal{B}}[I_s]$ is a constant matrix as seen from the $\mathcal{B}$ frame, even with the offcenter DGVSCMG inertia added [26]. The vector $\boldsymbol{\omega}_{\mathcal{B}/\mathcal{N}}$ is the inertial angular velocity of the spacecraft; and $\boldsymbol{\omega}_{\mathcal{G}_{oj}/\mathcal{N}}$, $\boldsymbol{\omega}_{\mathcal{G}_{ij}/\mathcal{N}}$, and $\boldsymbol{\omega}_{\mathcal{W}_j/\mathcal{N}}$ denote the jth inertia angular velocity of the outer gimbal, inner gimbal, and wheel, respectively. The EOM of a system of rigid bodies follows from Euler's equation [31] as follows:

$$ \dot{\boldsymbol{H}} = \boldsymbol{L} \tag{7} $$

where the vector $\boldsymbol{L}$ represents the sum of all the external torques experienced by the spacecraft. Substituting Eq. (4) into the left-hand side (LHS) of Eq. (7) yields

$$ \dot{\boldsymbol{H}}_B + \dot{\boldsymbol{H}}_{go} + \dot{\boldsymbol{H}}_{gi} + \dot{\boldsymbol{H}}_{ws} = \boldsymbol{L} \tag{8} $$

In the following development, the short-hand notation $\boldsymbol{\omega} = \boldsymbol{\omega}_{\mathcal{B}/\mathcal{N}}$ is used to make the equation description more compact. Similarly, gimbal frame angular velocity and wheel spin frame angular velocity definitions are shortened such as $\boldsymbol{\omega}_{\mathcal{G}_{oj}/\mathcal{N}} = \boldsymbol{\omega}_{goj}$, $\boldsymbol{\omega}_{\mathcal{G}_{ij}/\mathcal{N}} = \boldsymbol{\omega}_{gij}$ and $\omega_{\mathcal{W}_j/\mathcal{N}} = \omega_{wsj}$. Taking the inertial time derivative of the first term of the LHS in Eq. (8) leads to

$$ \dot{\boldsymbol{H}}_B = [I_s]\dot{\boldsymbol{\omega}} + \boldsymbol{\omega}^{\times}[I_s]\boldsymbol{\omega} \tag{9} $$

where notation $\boldsymbol{x}^{\times}$ denotes the following skew-symmetric matrix:

$$ \boldsymbol{x}^{\times} \coloneqq \begin{bmatrix} 0 & -x_3 & x_2 \\ x_3 & 0 & -x_1 \\ -x_2 & x_1 & 0 \end{bmatrix}, \qquad {}^{\forall}\boldsymbol{x} = [\,x_1 \quad x_2 \quad x_3\,]^T \tag{10} $$

The second term of the LHS in Eq. (8) is related to the outer gimbals of the DGVSCMGs. This is shown as follows:

$$ \dot{\boldsymbol{H}}_{go} = \sum_{j=1}^{n}\left(\frac{{}^{\mathcal{G}_{oj}}\mathrm{d}}{\mathrm{d}t}([I_{go}]\boldsymbol{\omega}_{goj}) + \boldsymbol{\omega}_{goj}^{\times}([I_{go}]\boldsymbol{\omega}_{goj})\right) \tag{11} $$

$$ = [I_{go}]\sum_{j=1}^{n}\left(\frac{{}^{\mathcal{N}}\mathrm{d}}{\mathrm{d}t}(\boldsymbol{\omega} + \dot{\delta}_{oj}\hat{\boldsymbol{g}}_{oj}) + \boldsymbol{\omega}_{goj}^{\times}([I_{go}]\boldsymbol{\omega}_{goj})\right) \tag{12} $$

$$ = [I_{go}]\sum_{j=1}^{n}\left(\dot{\boldsymbol{\omega}} + \ddot{\delta}_{oj}\hat{\boldsymbol{g}}_{oj} + \boldsymbol{\omega}^{\times}\left(\dot{\delta}_{oj}\hat{\boldsymbol{g}}_{oj}\right) + \boldsymbol{\omega}_{goj}^{\times}\left([I_{go}]\boldsymbol{\omega}_{goj}\right)\right) \tag{13} $$

$$ = n[I_{go}]\dot{\boldsymbol{\omega}} + [I_{go}]\left(G_{go}\ddot{\boldsymbol{\delta}}_o + \boldsymbol{\omega}^{\times}(G_{go}\dot{\boldsymbol{\delta}}_o)\right) + \sum_{j=1}^{n}\boldsymbol{\omega}_{goj}^{\times}\left([I_{go}]\boldsymbol{\omega}_{goj}\right) \tag{14} $$

where ${}^{i}\mathrm{d}/\mathrm{d}t$ is used to define a frame-dependent time derivative with respect to frame i, $\boldsymbol{\delta}_o = [\delta_{o1}, \cdots, \delta_{on}]^T \in R^{n\times 1}$ is the outer gimbal angle vector, and $G_{go} = [\hat{\boldsymbol{g}}_{o1}, \cdots, \hat{\boldsymbol{g}}_{on}] \in R^{3\times n}$ denotes the matrix of the outer gimbal axes. Note that $[I_{go}]$ is removed from the derivative in the second line because it is constant in the $\mathcal{G}_o$ frame. Similarly, the third term of the LHS in Eq. (8) is related to the inner gimbals of the DGVSCMGs. This is shown as follows:

$$ \begin{aligned} \dot{\boldsymbol{H}}_{gi} = {} & n[I_{gi}]\dot{\boldsymbol{\omega}} + [I_{gi}]\left(G_{go}\ddot{\boldsymbol{\delta}}_o + G_{gi}\ddot{\boldsymbol{\delta}}_i + \boldsymbol{\omega}^{\times}\left(G_{go}\dot{\boldsymbol{\delta}}_o + G_{gi}\dot{\boldsymbol{\delta}}_i\right)\right. \\ & \left. + \left(G_{go}\dot{\boldsymbol{\delta}}_o\right)^{\times}\left(G_{gi}\dot{\boldsymbol{\delta}}_i\right)\right) + \sum_{j=1}^{n}\boldsymbol{\omega}_{gij}^{\times}\left([I_{gi}]\boldsymbol{\omega}_{gij}\right) \end{aligned} \tag{15} $$

where $\boldsymbol{\delta}_i = [\delta_{i1}, \cdots, \delta_{in}]^T \in R^{n\times 1}$ is the inner gimbal angle vector, and $G_{gi} = [\hat{\boldsymbol{g}}_{i1}, \cdots, \hat{\boldsymbol{g}}_{in}] \in R^{3\times n}$ denotes the matrix of the inner gimbal axes. The fourth term of the LHS in Eq. (8) is related to the wheel spin rates of the DGVSCMGs. This is shown as follows:

$$ \begin{aligned} \dot{\boldsymbol{H}}_{ws} = {} & n[I_{ws}]\dot{\boldsymbol{\omega}} + [I_{ws}]\left(G_{go}\ddot{\boldsymbol{\delta}}_o + G_{gi}\ddot{\boldsymbol{\delta}}_i + G_{ws}\dot{\boldsymbol{\Omega}}\right. \\ & + \boldsymbol{\omega}^{\times}\left(G_{go}\dot{\boldsymbol{\delta}}_o + G_{gi}\dot{\boldsymbol{\delta}}_i + G_{ws}\boldsymbol{\Omega}\right) + \left(G_{go}\dot{\boldsymbol{\delta}}_o\right)^{\times}\left(G_{gi}\dot{\boldsymbol{\delta}}_i + G_{ws}\boldsymbol{\Omega}\right) \\ & \left. + \left(G_{gi}\dot{\boldsymbol{\delta}}_i\right)^{\times}(G_{ws}\boldsymbol{\Omega})\right) + \sum_{j=1}^{n}\boldsymbol{\omega}_{wsj}^{\times}\left([I_{ws}]\boldsymbol{\omega}_{wsj}\right) \end{aligned} \tag{16} $$

where $\boldsymbol{\Omega} = [\Omega_1, \cdots, \Omega_n]^T \in R^{n\times 1}$ is the wheel spin rate vector, and $G_{ws} = [\hat{\boldsymbol{s}}_1, \cdots, \hat{\boldsymbol{s}}_n] \in R^{3\times n}$ denotes the matrix of the spin axes. The total inertia matrix $[J]$ of a spacecraft including n DGVSCMGs is given by

$$ [J] = [I_s] + n\left([I_{go}] + [I_{gi}] + [I_{ws}]\right) \tag{17} $$

Note that this inertia tensor $[J]$ is not constant if taken in the body frame $\mathcal{B}$ by outer/inner gimbaling. In summary, Eq. (8) is rewritten as the final spacecraft/DGVSCMGs kinetic equations of motion:

$$
\begin{aligned}
[J]\dot{\boldsymbol{\omega}} = &-[I_{go}]\left(G_{go}\ddot{\boldsymbol{\delta}}_o + \boldsymbol{\omega}^{\times}\left(G_{go}\dot{\boldsymbol{\delta}}_o\right)\right)\\
&-[I_{gi}]\left(G_{go}\ddot{\boldsymbol{\delta}}_o + G_{gi}\ddot{\boldsymbol{\delta}}_i + \boldsymbol{\omega}^{\times}\left(G_{go}\dot{\boldsymbol{\delta}}_o + G_{gi}\dot{\boldsymbol{\delta}}_i\right) + \left(G_{gi}\dot{\boldsymbol{\delta}}_i\right)^{\times}\left(G_{go}\dot{\boldsymbol{\delta}}_o\right)\right)\\
&-[I_{ws}]\left(G_{go}\ddot{\boldsymbol{\delta}}_o + G_{gi}\ddot{\boldsymbol{\delta}}_i + G_{ws}\dot{\boldsymbol{\Omega}} + \boldsymbol{\omega}^{\times}\left(G_{go}\dot{\boldsymbol{\delta}}_o + G_{gi}\dot{\boldsymbol{\delta}}_i + G_{ws}\boldsymbol{\Omega}\right)\right.\\
&\left.+\left(G_{go}\dot{\boldsymbol{\delta}}_o\right)^{\times}\left(G_{gi}\dot{\boldsymbol{\delta}}_i + G_{ws}\boldsymbol{\Omega}\right) + \left(G_{gi}\dot{\boldsymbol{\delta}}_i\right)^{\times}\left(G_{ws}\boldsymbol{\Omega}\right)\right) - \boldsymbol{\omega}^{\times}[I_s]\boldsymbol{\omega}\\
&-\sum_{j=1}^{n}\left(\boldsymbol{\omega}_{wsj}^{\times}([I_{ws}]\boldsymbol{\omega}_{wsj}) + \boldsymbol{\omega}_{gij}^{\times}([I_{gi}]\boldsymbol{\omega}_{gij}) + \boldsymbol{\omega}_{goj}^{\times}([I_{go}]\boldsymbol{\omega}_{goj})\right) + \boldsymbol{L}
\end{aligned}
\tag{18}
$$

This is the kinetic EOM of a spacecraft with multiple DGVSCMGs.

III. LPV Model for Three-Axis Attitude Tracking

A. Linear Tracking Dynamics

This Paper deals with two parallel DGVSCMGs' allocation depicted as in Fig. 3. In this case, direction matrices in Eq. (18) are given by

$$
G_{go} = \begin{bmatrix} 0 & 0 \\ 0 & 0 \\ 1 & 1 \end{bmatrix}, \quad G_{gi} = \begin{bmatrix} -\sin\delta_{o1} & -\sin\delta_{o2} \\ \cos\delta_{o1} & \cos\delta_{o2} \\ 0 & 0 \end{bmatrix},
$$
$$
G_{ws} = \begin{bmatrix} \cos\delta_{i1}\cos\delta_{o1} & \cos\delta_{i2}\cos\delta_{o2} \\ \cos\delta_{i1}\sin\delta_{o1} & \cos\delta_{i2}\sin\delta_{o2} \\ -\sin\delta_{i1} & -\sin\delta_{i2} \end{bmatrix} \tag{19}
$$

To introduce the reference angular velocity vector $\boldsymbol{\omega}_{\mathcal{R}/\mathcal{N}}$ of the reference frame $\mathcal{R}$ relative to $\mathcal{N}$, the error angular velocity $\boldsymbol{\omega}_e$ and the inertial time derivative of $\boldsymbol{\omega}_e$ are given by

$$
\boldsymbol{\omega}_e = \boldsymbol{\omega} - \boldsymbol{\omega}_{\mathcal{R}/\mathcal{N}}, \quad \dot{\boldsymbol{\omega}}_e = \dot{\boldsymbol{\omega}} - \dot{\boldsymbol{\omega}}_{\mathcal{R}/\mathcal{N}} \tag{20}
$$

By using a Jacobian linearization of Eq. (18) around the equilibrium point ($\boldsymbol{\omega}_{e_{\text{eq}}} = 0$, $\dot{\boldsymbol{\Omega}}_{\text{eq}} = 0$, $\dot{\boldsymbol{\delta}}_{i_{\text{eq}}} = 0$, $\dot{\boldsymbol{\delta}}_{o_{\text{eq}}} = 0$) and introducing Eq. (20), the linear EOM of a spacecraft with DGVSCMGs is as follows:

$$
\dot{\boldsymbol{\omega}}_e = \boldsymbol{A}(\boldsymbol{\rho})\boldsymbol{\omega}_e + \boldsymbol{B}\boldsymbol{u} + Ew \tag{21}
$$

where

$$
\boldsymbol{A}(\boldsymbol{\rho}) = [J]^{-1}[I_{ws}](G_{ws}\boldsymbol{\Omega})^{\times} \tag{22}
$$

$$
\boldsymbol{B} = -[J]^{-1}[I_{ws}] \tag{23}
$$

Ew is the disturbance term including the model error, and $\boldsymbol{u}$ is the control input as follows:

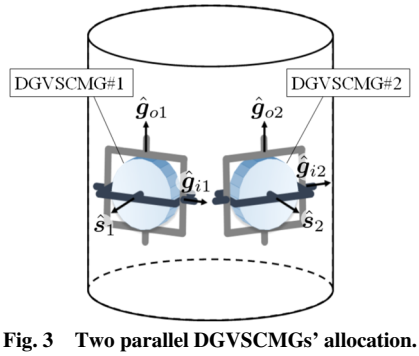

Fig. 3 Two parallel DGVSCMGs' allocation.

$$
\boldsymbol{u} = \begin{bmatrix} \boldsymbol{F}_{ws} & \boldsymbol{F}_{gi} & \boldsymbol{F}_{go} \end{bmatrix} \begin{bmatrix} \dot{\boldsymbol{\Omega}} \\ \dot{\boldsymbol{\delta}}_i \\ \dot{\boldsymbol{\delta}}_o \end{bmatrix} \tag{24}
$$

with

$$
\boldsymbol{F}_{ws} = \begin{bmatrix} \cos\delta_{i1}\cos\delta_{o1} & \cos\delta_{i2}\cos\delta_{o2} \\ \cos\delta_{i1}\sin\delta_{o1} & \cos\delta_{i2}\sin\delta_{o2} \\ -\sin\delta_{i1} & -\sin\delta_{i2} \end{bmatrix},
$$
$$
\boldsymbol{F}_{gi} = \begin{bmatrix} -\Omega_1\sin\delta_{i1}\cos\delta_{o1} & -\Omega_2\sin\delta_{i2}\cos\delta_{o2} \\ -\Omega_1\sin\delta_{i1}\sin\delta_{o1} & -\Omega_2\sin\delta_{i2}\sin\delta_{o2} \\ -\Omega_1\cos\delta_{i1} & -\Omega_2\cos\delta_{i2} \end{bmatrix},
$$
$$
\boldsymbol{F}_{go} = \begin{bmatrix} -\Omega_1\cos\delta_{i1}\sin\delta_{o1} & -\Omega_2\cos\delta_{i2}\sin\delta_{o2} \\ \Omega_1\cos\delta_{i1}\cos\delta_{o1} & \Omega_2\cos\delta_{i2}\cos\delta_{o2} \\ 0 & 0 \end{bmatrix} \tag{25}
$$

B. Linear Rigid-Body Kinematics

The spacecraft attitude is given by the orientation of the body-fixed frame $\mathcal{B}$ with respect to the inertial frame $\mathcal{N}$. It is known that three kinematic parameters are enough to describe the attitude. As such three kinematic parameters, in this Paper, modified Rodrigues parameters (MRPs) along with their shadow set are chosen [31,32]. They are a popular nonsingular attitude description with a minimal coordinate set by switching between the two possible MRP descriptions. They linearize very well, which is a benefit in the following discussion. However, other attitude coordinates could be used here as well without impacting the results. The MRP vector $\boldsymbol{\sigma}$ is defined in terms of the Euler parameters as the transformation

$$
\sigma_i = \frac{\beta_i}{1+\beta_0} \qquad i = 1,2,3 \tag{26}
$$

The inverse transformation is given by

$$
\beta_0 = \frac{1-\boldsymbol{\sigma}^T\boldsymbol{\sigma}}{1+\boldsymbol{\sigma}^T\boldsymbol{\sigma}}, \qquad \beta_i = \frac{2\sigma_i}{1+\boldsymbol{\sigma}^T\boldsymbol{\sigma}}, \qquad i = 1,2,3 \tag{27}
$$

Using the principal rotation axis vector $\hat{\boldsymbol{e}}$ and the rotation angle Φ, MRPs are given by

$$
\boldsymbol{\sigma} = \tan\left(\frac{\Phi}{4}\right)\hat{\boldsymbol{e}} \tag{28}
$$

For such MRPs, the singular points are given at $\Phi = \pm 2\pi$. However, these singularities can be avoided by introducing the dual MRP method that consists of the conventional MRP and the shadow MRP [31,32]. The kinematic equation based on the error MRPs $\boldsymbol{\sigma}_e$ is given by

$$
\dot{\boldsymbol{\sigma}}_e = \boldsymbol{H}(\boldsymbol{\sigma}_e)\boldsymbol{\omega}_e \tag{29a}
$$

$$
\boldsymbol{H}(\boldsymbol{\sigma}_e) = \frac{1}{4}\left[(1-\boldsymbol{\sigma}_e^T\boldsymbol{\sigma}_e)I_3 + 2\boldsymbol{\sigma}_e^{\times} + 2\boldsymbol{\sigma}_e\boldsymbol{\sigma}_e^T\right] \tag{29b}
$$

Let us transform Eq. (29) into an LPV model. The Jacobian linearization of Eq. (29) around the equilibrium point ($\boldsymbol{\omega}_{e_{\text{eq}}} = 0$, $\boldsymbol{\sigma}_{e_{\text{eq}}} = 0$) leads to the linearized kinematics with MRPs, which is given by

$$
\dot{\boldsymbol{\sigma}}_e \simeq \frac{1}{4}\boldsymbol{\omega}_e \tag{30}
$$

C. LPV Modeling

Setting the state variable $\boldsymbol{x} \coloneqq [\boldsymbol{\omega}_e^T \quad \boldsymbol{\sigma}_e^T]^T$, the state-space representation of Eqs. (21) and (30) is rewritten as follows:

$$\begin{bmatrix} \dot{\omega}_e \\ \dot{\sigma}_e \end{bmatrix} = \begin{bmatrix} \boldsymbol{A}(\boldsymbol{\rho}) & 0 \\ \frac{1}{4} I_3 & 0 \end{bmatrix} \begin{bmatrix} \boldsymbol{\omega}_e \\ \boldsymbol{\sigma}_e \end{bmatrix} + \begin{bmatrix} \boldsymbol{B} \\ 0 \end{bmatrix} \boldsymbol{u} + \begin{bmatrix} E \\ 0 \end{bmatrix} \boldsymbol{w} \tag{31}$$

which is equivalently written in a more compact formulation as

$$\dot{\boldsymbol{x}} = \boldsymbol{A}_e(\boldsymbol{\rho})\boldsymbol{x} + \boldsymbol{B}_e \boldsymbol{u} + E_e \boldsymbol{w} \tag{32}$$

The Jacobian matrices are defined as

$$\boldsymbol{A}_e(\boldsymbol{\rho}) \coloneqq \begin{bmatrix} \boldsymbol{A}(\boldsymbol{\rho}) & 0 \\ \frac{1}{4} I_3 & 0 \end{bmatrix}, \quad \boldsymbol{B}_e \coloneqq \begin{bmatrix} \boldsymbol{B} \\ 0 \end{bmatrix}, \quad E_e \coloneqq \begin{bmatrix} E \\ 0 \end{bmatrix} \tag{33}$$

with

$$\boldsymbol{\rho} = \begin{bmatrix} \rho_1 \\ \rho_2 \\ \rho_3 \end{bmatrix} \coloneqq G_{ws}\boldsymbol{\Omega} = \begin{bmatrix} \Omega_1 \cos\delta_{i1} \cos\delta_{o1} + \Omega_2 \cos\delta_{i2} \cos\delta_{o2} \\ \Omega_1 \cos\delta_{i1} \sin\delta_{o1} + \Omega_2 \cos\delta_{i2} \sin\delta_{o2} \\ -\Omega_1 \sin\delta_{i1} - \Omega_2 \sin\delta_{i2} \end{bmatrix} \tag{34}$$

It seems that the number of the scheduling parameters generally depends on the number of actuators. If it is true, it is difficult to design the GS controller to guarantee overall stability and control performance for a whole operating range of the LPV system because the number of LMIs to be solved simultaneously increases proportionally to the number of actuators. However, it is not true. By defining the scheduling parameters adequately as in Eq. (34), one can reduce the number of the scheduling parameters into just three, regardless of the number of actuators. This number is the same as the dimension of the spacecraft dynamics.

IV. Controller Design with Convex Optimization

A GS controller $\boldsymbol{K}(\boldsymbol{\rho})$ that guarantees overall stability and achieves mixed $\mathcal{H}_2/\mathcal{H}_\infty$ performance [15] for the LPV model as in Eq. (32) is considered. First, the generalized plant for Eq. (32) with the performance output vector $\boldsymbol{z}$ and the state-feedback controller are defined as follows:

$$\dot{\boldsymbol{x}} = \boldsymbol{A}_e(\boldsymbol{\rho})\boldsymbol{x} + \boldsymbol{B}_e \boldsymbol{u} + E_e \boldsymbol{w} \tag{35a}$$

$$\boldsymbol{z} = C\boldsymbol{x} + D\boldsymbol{u} \tag{35b}$$

$$\boldsymbol{u} = -K(\boldsymbol{\rho})\boldsymbol{x} \tag{35c}$$

where the coefficient matrix set (C, D) is selected such that they satisfy the condition $C^T D = 0$, $D^T D > 0$. The LPV system and the GS controller are expressed by the following polytopic representation:

$$\boldsymbol{A}_e(\boldsymbol{\rho}) = \sum_{i=1}^{p} \lambda_i(\boldsymbol{\rho}) \boldsymbol{A}_{ei} \tag{36}$$

$$\boldsymbol{K}(\boldsymbol{\rho}) = \sum_{i=1}^{p} \lambda_i(\boldsymbol{\rho}) \boldsymbol{K}_i \tag{37}$$

$$\lambda_i(\boldsymbol{\rho}) \geq 0, \qquad \sum_{i=1}^{p} \lambda_i(\boldsymbol{\rho}) = 1 \tag{38}$$

where p denotes the number of vertices. In this case, p is equal to $8(= 2^3)$ and $\lambda_i(\boldsymbol{\rho})$ is given as in Table 1. The scheduling parameter ρ_i in Eq. (34) has its upper and lower bounds, which are denoted by $\overline{\rho}_i$ and $\underline{\rho}_i$, respectively. They are given as follows:

Table 1 Convex combination coefficients

i	$\boldsymbol{\rho}$	$\lambda_i(\boldsymbol{\rho})$	Binary
1	$[\underline{\rho}_1 \quad \underline{\rho}_2 \quad \underline{\rho}_3]^T$	$\underline{\alpha}_1\underline{\alpha}_2\underline{\alpha}_3$	000
2	$[\underline{\rho}_1 \quad \underline{\rho}_2 \quad \overline{\rho}_3]^T$	$\underline{\alpha}_1\underline{\alpha}_2\overline{\alpha}_3$	001
3	$[\underline{\rho}_1 \quad \overline{\rho}_2 \quad \underline{\rho}_3]^T$	$\underline{\alpha}_1\overline{\alpha}_2\underline{\alpha}_3$	010
4	$[\underline{\rho}_1 \quad \overline{\rho}_2 \quad \overline{\rho}_3]^T$	$\underline{\alpha}_1\overline{\alpha}_2\overline{\alpha}_3$	011
5	$[\overline{\rho}_1 \quad \underline{\rho}_2 \quad \underline{\rho}_3]^T$	$\overline{\alpha}_1\underline{\alpha}_2\underline{\alpha}_3$	100
6	$[\overline{\rho}_1 \quad \underline{\rho}_2 \quad \overline{\rho}_3]^T$	$\overline{\alpha}_1\underline{\alpha}_2\overline{\alpha}_3$	101
7	$[\overline{\rho}_1 \quad \overline{\rho}_2 \quad \underline{\rho}_3]^T$	$\overline{\alpha}_1\overline{\alpha}_2\underline{\alpha}_3$	110
8	$[\overline{\rho}_1 \quad \overline{\rho}_2 \quad \overline{\rho}_3]^T$	$\overline{\alpha}_1\overline{\alpha}_2\overline{\alpha}_3$	111

$$\overline{\rho}_i = \Omega_{1\max} + \Omega_{2\max} \tag{39}$$

$$\underline{\rho}_i = -(\Omega_{1\max} + \Omega_{2\max}) \tag{40}$$

where $|\Omega_j| \leq \Omega_{j\max}$, $j = 1, 2$. Introducing interpolation parameters $\underline{\alpha}_i$ and $\overline{\alpha}_i$, the scheduling parameters ρ_i can be described as follows:

$$\rho_i = \underline{\alpha}_i\underline{\rho}_i + \overline{\alpha}_i\overline{\rho}_i, \quad 0 \leq \underline{\alpha}_i, \quad \overline{\alpha}_i \leq 1, \quad \underline{\alpha}_i + \overline{\alpha}_i = 1 \tag{41}$$

The extreme matrices $\boldsymbol{A}_{ei}$, $1 \leq i \leq p$ in Eq. (36) are given by any frozen system of $\boldsymbol{A}(\boldsymbol{\rho})$ with any combination of $\overline{\rho}_i$ and $\underline{\rho}_i$, as in Table 1. The extreme controllers $\boldsymbol{K}_{ei}$, $1 \leq i \leq p$ in Eq. (37) are designed for the extreme matrices $\boldsymbol{A}_{ei}$, $1 \leq i \leq p$ in Eq. (36), respectively. In this way, the convex hull that defines a whole operating range is constructed as shown in Fig. 4.

Let us introduce the following mixed $\mathcal{H}_2/\mathcal{H}_\infty$ LMI problem [15]:

$$\inf_{W_i, X, Z} [\mathrm{Trace}(\boldsymbol{Z})] \tag{42a}$$

subject to

$$\begin{bmatrix} \boldsymbol{X} & * \\ E_e^T & \boldsymbol{Z} \end{bmatrix} > 0, \qquad \begin{bmatrix} (\boldsymbol{A}_{ei}\boldsymbol{X} - \boldsymbol{B}_e\boldsymbol{W}_i) + (\bullet)^T & * \\ C\boldsymbol{X} - D\boldsymbol{W}_i & -I \end{bmatrix} < 0 \tag{42b}$$

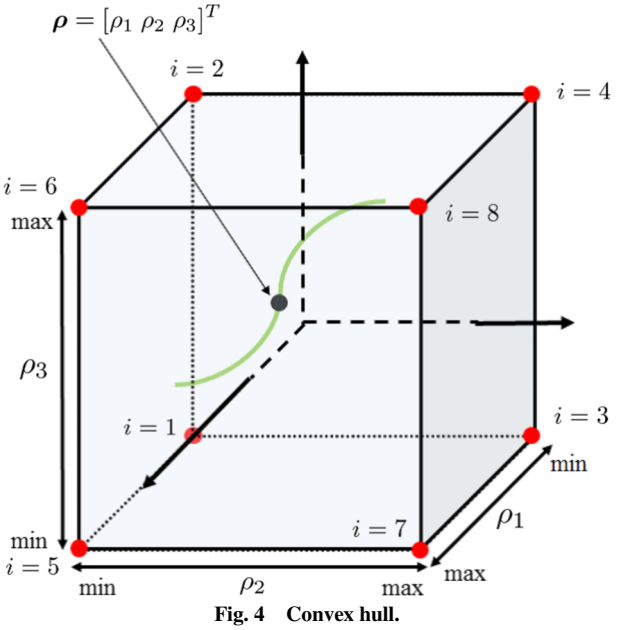

Fig. 4 Convex hull.

$$\begin{bmatrix} (\boldsymbol{A}_{ei}\boldsymbol{X} - \boldsymbol{B}_e\boldsymbol{W}_i) + (\bullet)^T & * & * \\ C\boldsymbol{X} - D\boldsymbol{W}_i & -\gamma I & * \\ E_e^T & 0 & -\gamma I \end{bmatrix} < 0,$$

$$\text{for all } 1 \le i \le p \tag{42c}$$

where $\boldsymbol{X} \in \boldsymbol{R}^{6\times6}$ and $\boldsymbol{W} \in \boldsymbol{R}^{3\times6}$ are matrix variables, and $\boldsymbol{Z} \in \boldsymbol{R}^{3\times3}$ is a slack variable. Equations (42a) and (42b) guarantee $\mathcal{H}_2$ performance, and Eq. (42c) gives $\mathcal{H}_\infty$ constraint. Using the optimal solution sets $\boldsymbol{X}$ and $\boldsymbol{W}_i$ to the problem in Eqs. (42), the extreme controllers $\boldsymbol{K}_i$ at each vertex of the operation range [9] are given by

$$\boldsymbol{K}_i = \boldsymbol{W}_i\boldsymbol{X}^{-1}, \quad 1 \le i \le p \tag{43}$$

Then, the GS controller in Eq. (35c) is constructed by substituting Eq. (43) into Eq. (37).

V. Steering Law Design

In [3–6], the IPACS with multiple reaction wheels or variable-speed CMG were developed. In this Paper, the IPACS with multiple DGVSCMGs is considered. Two types of steering laws for two parallel DGVSCMGs are proposed.

A. Steering Law 1

The first proposed steering law consists of RW steering and CMG steering.

1. RW Steering

Both power tracking and wheel spin equalization are attained by RW steering. First of all, the kinetic energy and power of RWs are considered. The kinetic energy of RWs in DGVSCMGs is given by

$$T_{\mathrm{RW}} = \frac{1}{2}\sum_{j=1}^{n} I_{wsj,x}\Omega_j^2 \tag{44}$$

Therefore, the power of RWs described as the rates of change of the energy is given by

$$P_{\mathrm{RW}} = \dot{T}_{\mathrm{RW}} = \sum_{j=1}^{n} I_{wsj,x}\Omega_j\dot{\Omega}_j = I_{ws,x}\boldsymbol{\Omega}^T\dot{\boldsymbol{\Omega}} \tag{45}$$

Note that the wheel inertias of all DGVSCMGs are assumed to be same as the wheel spin directions. Next, the RW steering law to attain the power tracking is considered. To introduce the required power P_r, the steering law of RWs is described as follows:

$$P_r = \tilde{\boldsymbol{P}}\dot{\boldsymbol{\Omega}}, \qquad \tilde{\boldsymbol{P}} = I_{ws,x}\boldsymbol{\Omega}^T \tag{46}$$

Therefore, the required inputs of the RWs are obtained to solve Eq. (46) as follows:

$$\dot{\boldsymbol{\Omega}} = \tilde{\boldsymbol{P}}^{\dagger}P_r + N_1M_1\boldsymbol{\Omega}_e \tag{47}$$

where

$$N_1 = I_2 - \tilde{\boldsymbol{P}}^{\dagger}\tilde{\boldsymbol{P}} \tag{48}$$

$$M_1 = k_1I_2 \tag{49}$$

$$\boldsymbol{\Omega}_e = \boldsymbol{\Omega} - \overline{\Omega}1_{2\times1} \tag{50}$$

$$\overline{\Omega} = \frac{1}{2}\sum_{i=1}^{2}\Omega_i \tag{51}$$

Note that matrix N_1 is the null motion of the RW steering law, M_1 is the weighting matrix, and $\boldsymbol{\Omega}_e$ is the error wheel spin rate vector to attain the wheel spin equalization in the null motion. The RW steering law in Eq. (47) can attain both power tracking and wheel spin equalization. Recalling that the control input $\boldsymbol{u}$ is given as in Eq. (24), the output torque vector of the RWs $\boldsymbol{u}_{\mathrm{RW}}$ is given by

$$\boldsymbol{u}_{\mathrm{RW}} = \boldsymbol{F}_{ws}\dot{\boldsymbol{\Omega}} \tag{52}$$

2. CMG Steering

Both three-axis attitude control and singularity avoidance are attained by CMG steering. The required CMG torque vector is calculated as follows:

$$\boldsymbol{u}_{\mathrm{CMG}} = \boldsymbol{u} - \boldsymbol{u}_{\mathrm{RW}} \tag{53}$$

Then, the CMG steering law is given by

$$\boldsymbol{u}_{\mathrm{CMG}} = Q\dot{\delta} \tag{54}$$

where

$$Q = \begin{bmatrix} \boldsymbol{F}_{gi} & \boldsymbol{F}_{go} \end{bmatrix}, \quad \dot{\boldsymbol{\delta}} = \begin{bmatrix} \dot{\boldsymbol{\delta}}_i \\ \dot{\boldsymbol{\delta}}_o \end{bmatrix} \tag{55}$$

If $\det(QQ^T) = 3$, Eq. (54) can be always solved with respect to $\dot{\boldsymbol{\delta}}$ for any given torque command $\boldsymbol{u}_{\mathrm{CMG}}$. If rank $(Q) \neq 3$, then this cannot be solved. It occurs when $\det(QQ^T) = 0$. The singularity measure m is introduced by

$$m = \sqrt{\det(QQ^T)} \tag{56}$$

When m is close to zero, the system falls into the singularity. The singularity robustness (SR) steering law [19] is one of the most efficient singularity avoidance techniques. Reference [21] gives an SR-based singular value decomposition (SVD) method that hires orthonormal matrices $U \in \boldsymbol{R}^{3\times3}$ and $V \in \boldsymbol{R}^{4\times4}$. In Eq. (54), the matrix Q can be decomposed into

$$Q = U\boldsymbol{\Sigma}V^T \tag{57}$$

where

$$\boldsymbol{\Sigma} = \begin{bmatrix} \overline{\sigma}_1 & 0 & 0 & 0 \\ 0 & \overline{\sigma}_2 & 0 & 0 \\ 0 & 0 & \overline{\sigma}_3 & 0 \end{bmatrix}, \quad U = [\overline{\boldsymbol{u}}_1 \ \ \overline{\boldsymbol{u}}_2 \ \ \overline{\boldsymbol{u}}_3], \quad V = [\boldsymbol{v}_1 \ \ \boldsymbol{v}_2 \ \ \boldsymbol{v}_3 \ \ \boldsymbol{v}_4] \tag{58}$$

that yields

$$Q = \sum_{i=1}^{3}\overline{\sigma}_i\overline{\boldsymbol{u}}_i\boldsymbol{v}_i^T \tag{59}$$

where $\overline{\sigma}_1 \ge \overline{\sigma}_2 \ge \overline{\sigma}_3 \ge 0$ are singular values of Q. If $\det(QQ^T) \neq 0$, then $\overline{\sigma}_i > 0$, $1 \le i \le 3$ and

$$Q^{\dagger} = V\boldsymbol{\Sigma}^{\dagger}U^T \tag{60}$$

where

$$\boldsymbol{\Sigma}^{\dagger} = \begin{bmatrix} \frac{1}{\overline{\sigma}_1} & 0 & 0 \\ 0 & \frac{1}{\overline{\sigma}_2} & 0 \\ 0 & 0 & \frac{1}{\overline{\sigma}_3} \\ 0 & 0 & 0 \end{bmatrix} \tag{61}$$

that yields

$$Q^{\dagger} = \sum_{i=1}^{3} \left(\frac{1}{\bar{\sigma}_i}\right) \boldsymbol{v}_i \bar{\boldsymbol{u}}_i^T \tag{62}$$

The SR inverse $Q^{\#} = Q^T[QQ^T + \lambda I_3]^{-1}$ is given as follows [21]:

$$N^{\#} = V\boldsymbol{\Sigma}^{\#}U^T \tag{63}$$

where

$$\boldsymbol{\Sigma}^{\#} = \begin{bmatrix} \frac{\bar{\sigma}_1}{\bar{\sigma}_1^2+\lambda} & 0 & 0 \\ 0 & \frac{\bar{\sigma}_2}{\bar{\sigma}_2^2+\lambda} & 0 \\ 0 & 0 & \frac{\bar{\sigma}_3}{\bar{\sigma}_3^2+\lambda} \\ 0 & 0 & 0 \end{bmatrix} \tag{64}$$

$$\lambda = k_2 \frac{1 - \exp[-(1/m)]}{1 + \exp[-(1/m)]} \tag{65}$$

where λ is the sigmoid function with positive scalar k_2 and singularity measure m. When the system is closed to the singularity, λ is approaching to k_2. Therefore, the SR-based SVD steering law is given by

$$\dot{\boldsymbol{\delta}} = Q^{\#}\boldsymbol{u}_{\mathrm{CMG}} \tag{66}$$

where

$$Q^{\#} = \sum_{i=1}^{3} \left(\frac{\bar{\sigma}_i}{\bar{\sigma}_i^2 + \lambda}\right) \boldsymbol{v}_i \bar{\boldsymbol{u}}_i^T \tag{67}$$

Although this steering law can avoid the singularity, it cannot escape from the singularity. Then, a singularity escape steering law is proposed as follows:

$$\dot{\boldsymbol{\delta}} = Q^{\#}\boldsymbol{u}_{\mathrm{CMG}} + N_2 M_2 \boldsymbol{v}_1 \tag{68}$$

where

$$N_2 = I_4 - Q^{\#}Q \tag{69}$$

$$M_2 = \lambda I_4 \tag{70}$$

where the matrix N_2 is the null motion of the CMG steering law, and M_2 is the weighting matrix with sigmoid function λ of singularity measure m. Vector $\boldsymbol{v}_1$ is employed to output the maximum torque in the direction orthogonal to the singularity surface and to escape rapidly from the singular point [33]. Figure 5 shows the procedure of the steering law computation. From this figure, the required torque $\boldsymbol{u}$ from the GS controller is divided into the wheel input $\boldsymbol{u}_{\mathrm{RW}}$ and the inner/outer gimbal input $\boldsymbol{u}_{\mathrm{CMG}}$. Note that the control performance of the thee-axis attitude control is guaranteed because the total generated torque amount in the three-dimensional motion is conserved.

B. Steering Law 2

This steering law provides three-axis attitude control, singularity avoidance, wheel spin equalization, and power tracking at the same time. The following steering law is considered as follows:

$$\begin{bmatrix} \boldsymbol{u} \\ P_r \end{bmatrix} = S \begin{bmatrix} \dot{\boldsymbol{\Omega}} \\ \dot{\boldsymbol{\delta}} \end{bmatrix} \tag{71}$$

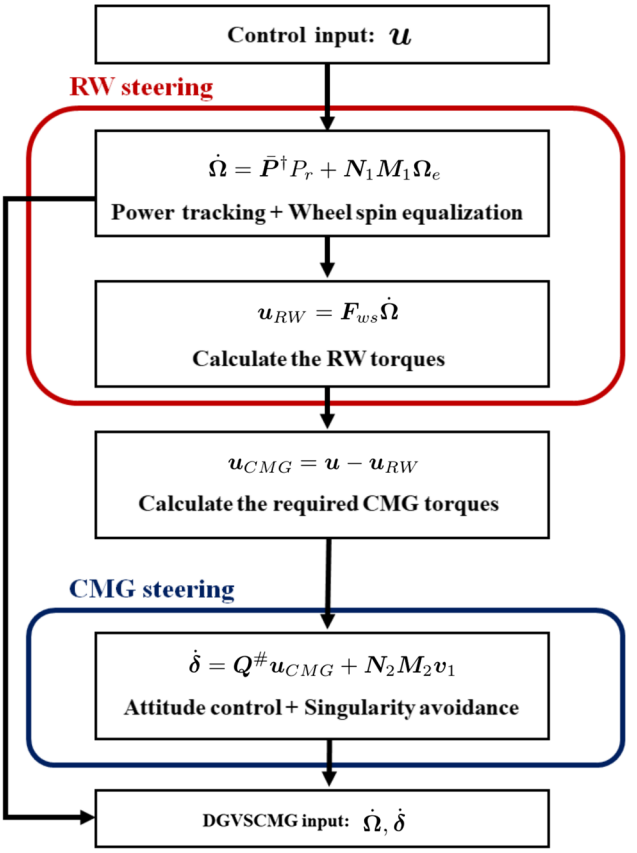

Fig. 5 Procedure of the steering computation.

where

$$S = \begin{bmatrix} \boldsymbol{F}_{ws} & Q \\ \bar{\boldsymbol{P}} & 0 \end{bmatrix} \tag{72}$$

The coefficient matrix S can be decomposed into

$$S = \tilde{U}\tilde{\boldsymbol{\Sigma}}\tilde{V}^T \tag{73}$$

where

$$\tilde{\boldsymbol{\Sigma}} = \begin{bmatrix} \tilde{\sigma}_1 & 0 & 0 & 0 & 0 & 0 \\ 0 & \tilde{\sigma}_2 & 0 & 0 & 0 & 0 \\ 0 & 0 & \tilde{\sigma}_3 & 0 & 0 & 0 \\ 0 & 0 & 0 & \tilde{\sigma}_4 & 0 & 0 \end{bmatrix}, \quad \tilde{U} = \begin{bmatrix} \tilde{\boldsymbol{u}}_1 & \tilde{\boldsymbol{u}}_2 & \tilde{\boldsymbol{u}}_3 & \tilde{\boldsymbol{u}}_4 \end{bmatrix},$$

$$\tilde{V} = \begin{bmatrix} \tilde{\boldsymbol{v}}_1 & \tilde{\boldsymbol{v}}_2 & \tilde{\boldsymbol{v}}_3 & \tilde{\boldsymbol{v}}_4 & \tilde{\boldsymbol{v}}_5 & \tilde{\boldsymbol{v}}_6 \end{bmatrix} \tag{74}$$

with

$$\tilde{\sigma}_1 \geq \tilde{\sigma}_2 \geq \tilde{\sigma}_3 \geq \tilde{\sigma}_4 \geq 0$$

that yields

$$S = \sum_{i=1}^{4} \tilde{\sigma}_i \tilde{\boldsymbol{u}}_i \tilde{\boldsymbol{v}}_i^T \tag{75}$$

To solve this equation, the DGVSCMG inputs are given by

$$\begin{bmatrix} \dot{\boldsymbol{\Omega}} \\ \dot{\boldsymbol{\delta}} \end{bmatrix} = S^{\#} \begin{bmatrix} \boldsymbol{u} \\ P_r \end{bmatrix} + N_3 \left(M_3 \begin{bmatrix} \boldsymbol{\Omega}_e \\ 0 \end{bmatrix} + M_4 \tilde{\boldsymbol{v}}_1 \right) \tag{76}$$

Table 2 Simulation parameters

Parameter	Value	Unit
${}^{\mathcal{B}}[I_s]$	diag [600 600 475]	kg/m^2
${}^{\mathcal{G}_i}[I_{ws}]$	diag [0.7 0.4 0.4]	kg/m^2
${}^{\mathcal{G}_i}[I_{gi}]$	diag [0.1 0.1 0.1]	kg/m^2
${}^{\mathcal{G}_o}[I_{go}]$	diag [0.1 0.1 0.1]	kg/m^2
$\boldsymbol{\Omega}_0$	$[650 \quad 600]^T$	rad/s
$\boldsymbol{\Omega}_{\max}$	$[750 \quad 750]^T$	rad/s
$\dot{\boldsymbol{\Omega}}_{\max}$	$[1 \quad 1]^T$	rad/s^2
$\dot{\boldsymbol{\Omega}}_{\min}$	$[-1 \quad -1]^T$	rad/s^2
$\boldsymbol{\delta}_0$	$[\pi/4 \quad -\pi/4 \quad 0 \quad \pi/2]^T$	rad
$\dot{\boldsymbol{\delta}}_{\max}$	$[1 \quad 1 \quad 1 \quad 1]^T$	rad/s
$\dot{\boldsymbol{\delta}}_{\min}$	$[-1 \quad -1 \quad -1 \quad -1]^T$	rad/s
$\boldsymbol{\omega}_{e0}$	$[0.003 \quad -0.005 \quad -0.025]^T$	rad/s
$\boldsymbol{\sigma}_{e0}$	$[0.2 \quad -0.2 \quad -0.6]^T$	— —

where

$$S^{\#} = \sum_{i=1}^{3} \left(\frac{\tilde{\sigma}_i}{\tilde{\sigma}_i^2 + \lambda} \right) \tilde{\boldsymbol{v}}_i \tilde{\boldsymbol{u}}_i^T \tag{77}$$

$$N_3 = I_6 - S^{\#} S \tag{78}$$

$$M_3 = k_1 I_6 \tag{79}$$

$$M_4 = \lambda I_6 \tag{80}$$

VI. Numerical Simulation

This section presents a numerical simulation of the attitude tracking problem given by the satellite in a near-polar orbit found in [3,4]. The pointing axis is required to track a ground station, and the spacecraft is required to rotate about this pointing vector so that the solar panel axis is perpendicular to the spacecraft–sun axis. These two constraints determine the required angular velocity for three-axis attitude control on orbit. Two numerical simulations using steering law 1 in Eq. (68) and steering law 2 in Eq. (76) are presented. The disturbance torque [34] experienced by aerodynamics, solar pressure, magnetic torque, and other environmental factors is assumed by

$$\boldsymbol{L} = \begin{bmatrix} 4 \times 10^{-6} + 2 \times 10^{-6} \sin(\overline{n}t) \\ 6 \times 10^{-6} + 3 \times 10^{-6} \sin(\overline{n}t) \\ 3 \times 10^{-6} + 3 \times 10^{-6} \sin(\overline{n}t) \end{bmatrix} \tag{81}$$

where $\overline{n}$ denotes mean motion. The controller design parameters C and D, the disturbance coefficient matrix E_e, and positive scalars k_1 and k_2 are given as follows:

$$C = \begin{bmatrix} 20 \times I_3 & 0_{3\times3} \\ 0_{3\times3} & 0.01 \times I_3 \\ 0_{3\times3} & 0_{3\times3} \end{bmatrix}, \quad D = \begin{bmatrix} 0_{6\times3} \\ 0.03 \times I_3 \end{bmatrix},$$

$$E_e = \begin{bmatrix} 10^{-6} \times \mathrm{diag}[6 \quad 9 \quad 6] \\ 0_{3\times3} \end{bmatrix} \tag{82}$$

$$k_1 = 0.2, \qquad k_2 = 10 \tag{83}$$

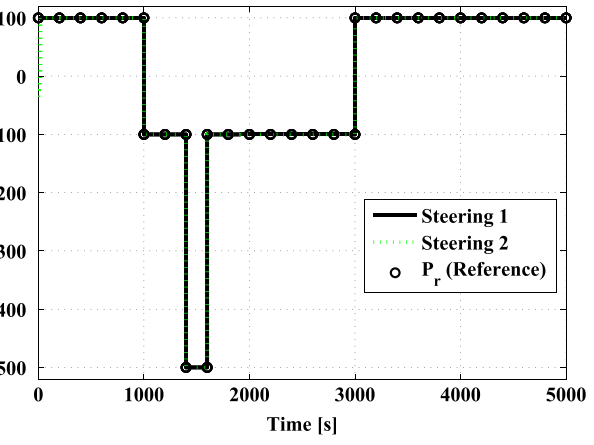

Fig. 6 Power profiles.

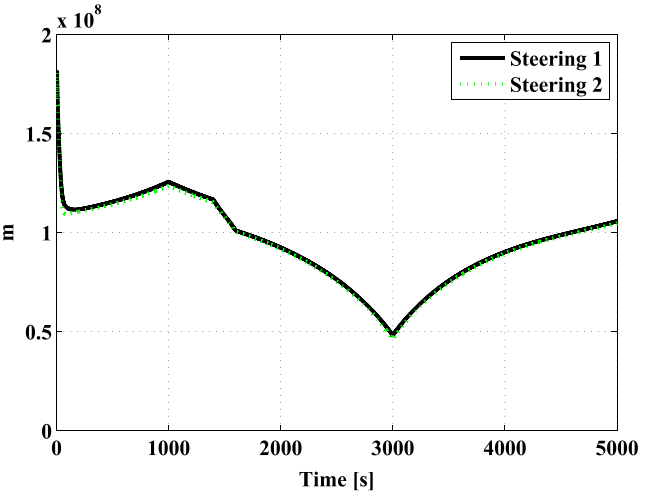

Fig. 7 Singularity measure.

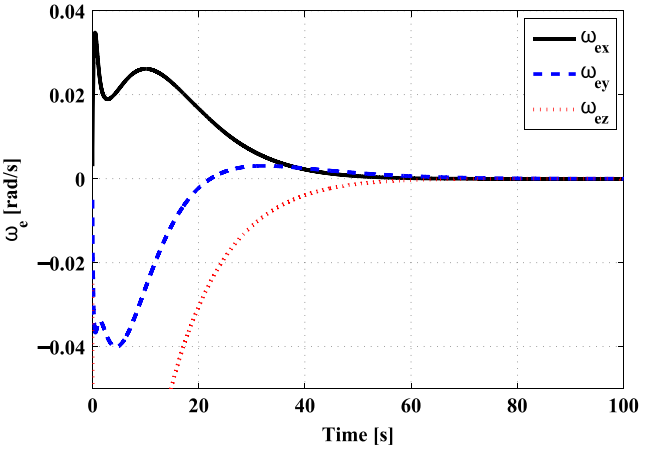

Fig. 8 Angular velocity (magnified).

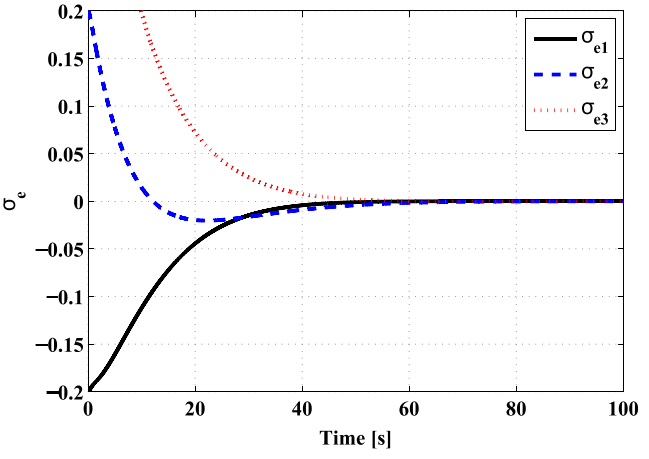

Fig. 9 Error MRPs (magnified).

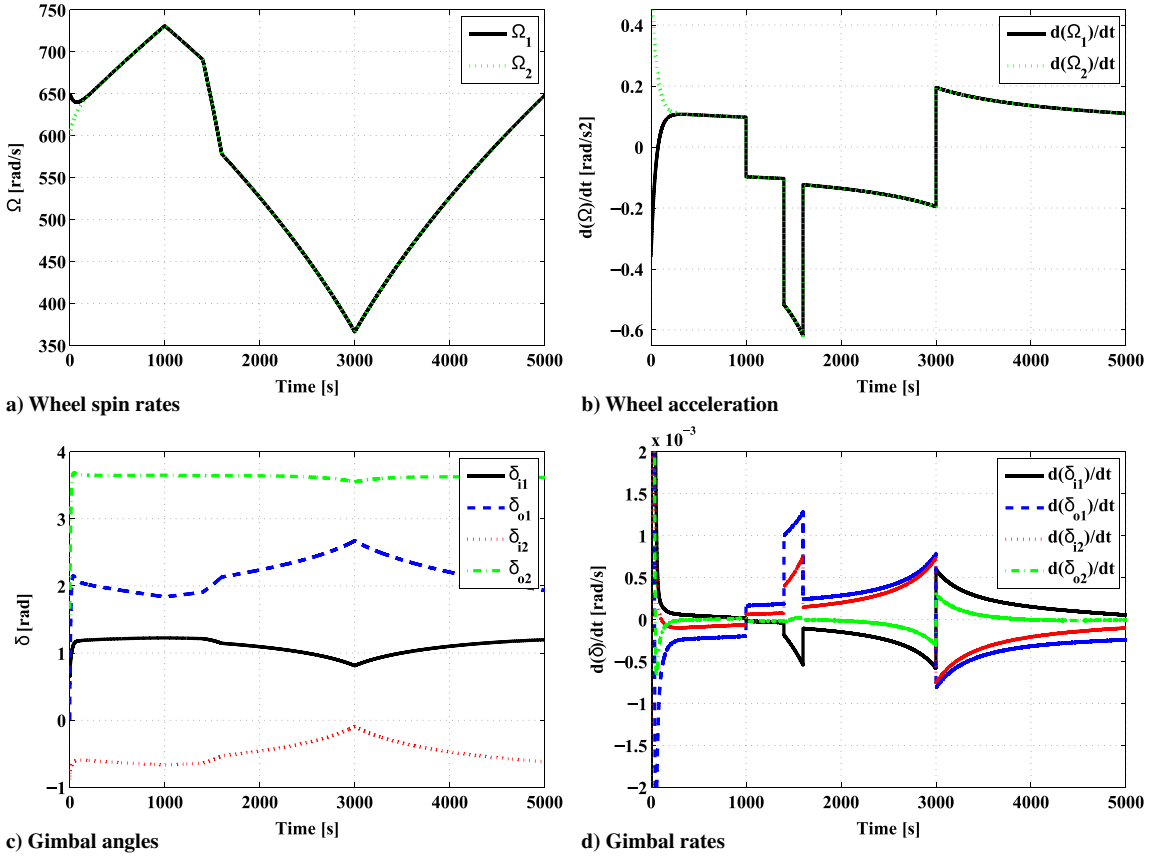

a) Wheel spin rates b) Wheel acceleration

c) Gimbal angles d) Gimbal rates

Fig. 10 Attitude and power tracking simulation (steering law 1).

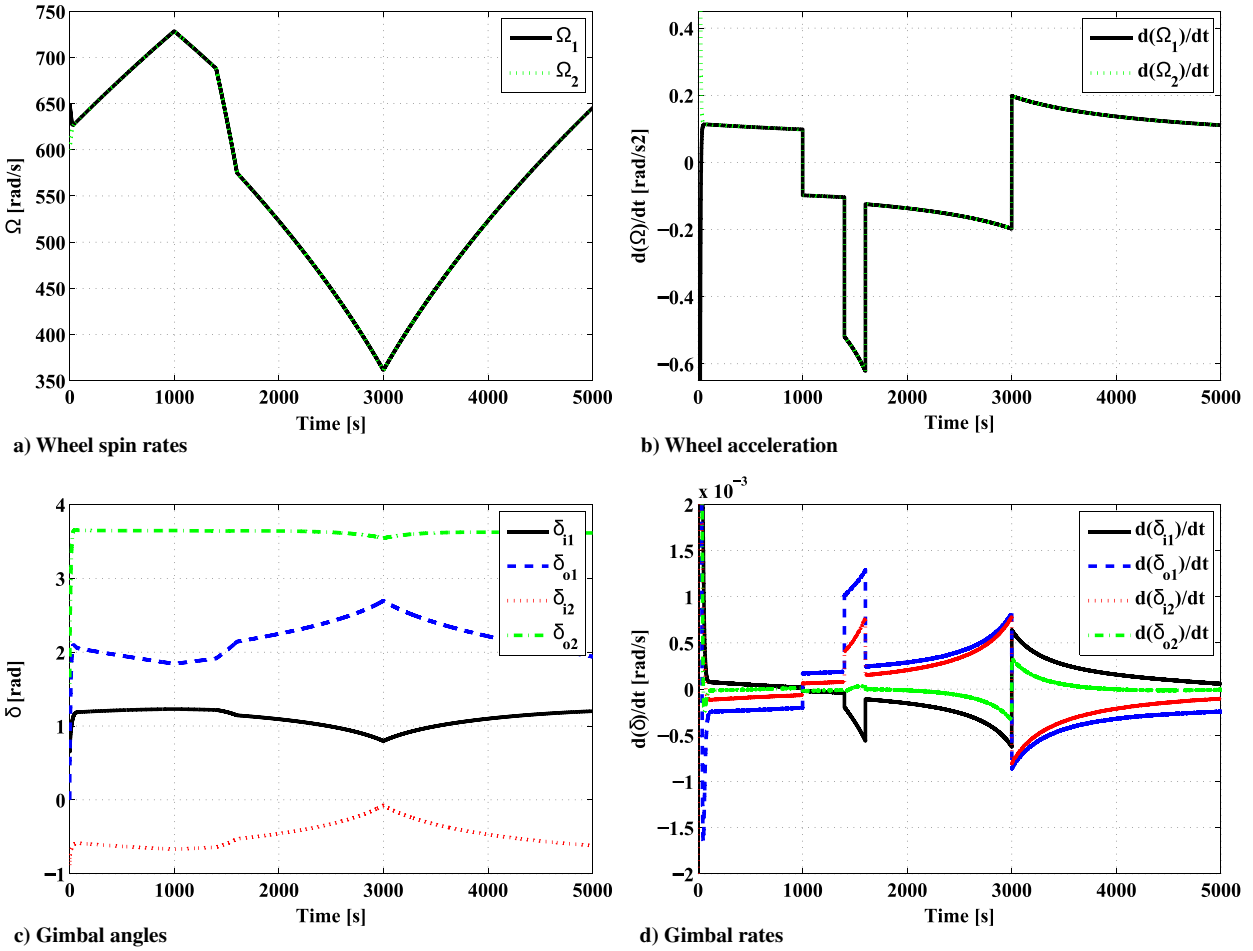

a) Wheel spin rates b) Wheel acceleration

c) Gimbal angles d) Gimbal rates

Fig. 11 Attitude and power tracking simulation (steering law 2).

Note that the disturbance coefficient matrix E_e is determined by the maximum values of the disturbance in Eq. (81). The simulation parameters are given in Table 2, in which the initial condition of the MRPs and the angular velocity of the spacecraft ($\boldsymbol{\sigma}_0$, $\boldsymbol{\omega}_0$) are also given. These spacecraft parameters closely parallel those used in [6,23]. The maximum and minimum values of the scheduling parameter in Eqs. (39) and (40) are given by $-1500 \leq \rho_i \leq 1500$ from the maximum wheel spin rates in Table 2.

Figure 6 shows the power history of the RWs in the DGVSCMGs, and Fig. 7 shows the singularity measure of the DGCMGs in the DGVSCMGs. From these figures, the power (the solid and dashed lines) are tracked by the required power (circles) in Fig. 6 and the singularity measure (the solid and dashed lines) in Fig. 7 avoided the singularity (it avoided 0). As a result, the proposed controller and the steering laws have achieved both power tracking and singularity avoidance. Figures 8 and 9 show the error angular velocity and the error MRPs, which are converged to 0 at 70 s. Therefore, the IPACS has been successfully achieved by the proposed control and steering laws.

Figures 10 and 11 show the simulation results of the DGVSCMG motion by using the steering laws in Eqs. (68) and (76), respectively. From these figures, the wheel motions in Figs. 10a, 10b, 11a, and 11b show that wheel spin equalization has been attained. With regard to the computing speed, steering law 2 is 1.12 times faster than steering law 1.

VII. Conclusions

In this Paper, the dynamics and linear parameter-varying model of a spacecraft equipped with multiple DGVSCMGs has been developed. Then, a multiobjective gain-scheduled controller with linear parameter-varying control theory was applied to evaluate both optimality and robustness. Two types of steering laws for two parallel DGVSCMGs were proposed to attain power tracking while considering both singularity avoidance and wheel spin equalization. Through numerical examples, an integrated power/attitude control system and the effectiveness of the proposed controller and steering laws were demonstrated. Also, the advantage of the computing speed was demonstrated by comparing two steering laws.

Acknowledgments

This work was supported by Japan Society for the Promotion of Science (JSPS) Grant-in-Aid for Scientific Research, grant numbers 15J11371 and (C)15K06149.

References

[1] Rose, J. B., "An Electro-Mechanics Energy Storage System for Space Application," *Progress in Astronautics and Rocketry*, Vol. 3, Academic Press, New York, 1961, pp. 613–622.

[2] Cormack, A., III, "Three Axis Flywheel Energy and Control Systems," NASA TN-73-G&C-8, 1973.

[3] Tsiotras, P., Shen, H., and Hall, C., "Satellite Attitude Control and Power Tracking with Energy/Momentum Wheels," *Journal of Guidance, Control, and Dynamics*, Vol. 24, No. 1, Jan.–Feb. 2001, pp. 23–34. doi:10.2514/2.4705

[4] Yoon, H., and Tsiotras, P., "Spacecraft Adaptive Attitude and Power Tracking with Variable Speed Control Moment Gyroscopes," *Journal of Guidance, Control, and Dynamics*, Vol. 25, No. 6, Nov.–Dec. 2002, pp. 1081–1090. doi:10.2514/2.4987

[5] Jung, D., and Tsiotras, P., "An Experimental Validation of Spacecraft Attitude and Power Tracking with Variable Speed Control Moment Gyroscopes," *17th AAS/AIAA Space Flight Mechanics Meeting*, AAS Paper 07-130, Sedona, AZ, Jan.–Feb. 2007.

[6] Park, J., and Palazzolo, A., "Magnetically Suspended VSCMGs for Simultaneous Attitude Control and Power Transfer IPAC Service," *Journal of Dynamic Systems, Measurement, and Control*, Vol. 132, No. 5, Sept. 2010, Paper 051001. doi:10.1115/1.4002105

[7] Tsiotras, P., "Stabilization and Optimality Results for the Attitude Control Problem," *Journal of Guidance, Control, and Dynamics*, Vol. 19, No. 4, July–Aug. 1996, pp. 772–779. doi:10.2514/3.21698

[8] Yoon, H., and Tsiotras, P., "Spacecraft Line-of-Sight Control Using a Single Variable-Speed Control Moment Gyro," *Journal of Guidance, Control, and Dynamics*, Vol. 29, No. 6, Nov.–Dec. 2006, pp. 1295–1308. doi:10.2514/1.18777

[9] Apkarian, P., Gahinet, P., and Becker, G., "Self-Scheduled $\mathcal{H}_\infty$ Control of Linear Parameter-Varying Systems: A Design Example," *Automatica*, Vol. 31, No. 9, Sept. 1995, pp. 1251–1261. doi:10.1016/0005-1098(95)00038-X

[10] Boyd, S., Ghaoui, E. L., Feron, E., and Balakrishnan, V., *Linear Matrix Inequalities in System and Control Theory*, Vol. 15, Studies in Applied Mathematics, Soc. for Industrial and Applied Mathematics, Philadelphia, PA, 1994, pp. 7–12. doi:10.1137/1.9781611970777

[11] Geromel, C. J., Peres, L. D. P., and Bernussou, J., "On a Convex Parameter Space Method for Linear Control Design of Uncertain Systems," *SIAM Journal on Control and Optimization*, Vol. 29, No. 2, 1991, pp. 381–402. doi:10.1137/0329021

[12] Masubuchi, I., Ohara, A., and Suda, N., "LMI-Based Controller Synthesis: A Unified Formulation and Solution," *International Journal of Robust and Nonlinear Control*, Vol. 8, No. 8, July 1998, pp. 669–686. doi:10.1002/(ISSN)1099-1239

[13] Kwon, S., Shimomura, T., and Okubo, H., "Pointing Control of Spacecraft Using Two SGCMGs via LPV Control Theory," *Acta Astronautica*, Vol. 68, Nos. 7–8, 2011, pp. 1168–1175. doi:10.1016/j.actaastro.2010.10.001

[14] Yamamoto, Y., and Shimomura, T., "Attitude Control of Spacecraft Through a Simple LPV Model with a Virtual State Variable," *AIAA Guidance, Navigation, and Control Conference*, AIAA Paper 2012-5005, 2012. doi:10.2514/6.2012-5005

[15] Khargonekar, P. P., and Rotea, M. A., "Mixed $\mathcal{H}_2/\mathcal{H}_\infty$ Control: A Convex Optimization Approach," *IEEE Transactions on Automatic Control*, Vol. 36, No. 7, 1991, pp. 824–837. doi:10.1109/9.85062

[16] Scherer, C., Gahinet, P., and Chilali, M., "Multiobjective Output-Feedback Control via LMI Optimization," *IEEE Transactions on Automatic Control*, Vol. 42, No. 7, July 1997, pp. 896–911. doi:10.1109/9.599969

[17] Schaub, H., and Lappas, J. V., "Redundant Reaction Wheel Torque Distribution Yielding Instantaneous L_2 Power-Optimal Attitude Control," *Journal of Guidance, Control, and Dynamics*, Vol. 32, No. 4, July–Aug. 2009, pp. 1269–1276. doi:10.2514/1.41070

[18] Blenden, R., and Schaub, H., "Regenerative Power-Optimal Reaction Wheel Attitude Control," *Journal of Guidance, Control, and Dynamics*, Vol. 35, No. 4, July–Aug. 2012, pp. 1208–1217. doi:10.2514/1.55493

[19] Wie, B., Bailey, D., and Heiberg, C., "Singularity Robust Steering Logic for Redundant Single-Gimbal Control Moment Gyros," *Journal of Guidance, Control, and Dynamics*, Vol. 24, No. 5, Sept.–Oct. 2001, pp. 865–872. doi:10.2514/2.4799

[20] Kurokawa, H., "Survey of Theory and Steering Laws of Single-Gimbal Control Moment Gyros," *Journal of Guidance, Control, and Dynamics*, Vol. 30, No. 5, Sept.–Oct. 2007, pp. 1331–1340. doi:10.2514/1.27316

[21] Ford, K. A., and Hall, C. D., "Singular Direction Avoidance Steering for Control Moment Gyros," *Journal of Guidance, Control, and Dynamics*, Vol. 23, No. 4, 2000, pp. 648–656. doi:10.2514/2.4610

[22] Yoon, H., and Tsiotras, P., "Singularity Analysis of Variable-Speed Control Moment Gyros," *Journal of Guidance, Control, and Dynamics*, Vol. 27, No. 3, May–June 2004, pp. 374–386. doi:10.2514/1.2946

[23] Schaub, H., Vadali, R. S., and Junkins, L. J., "Feedback Control Law for Variable Speed Control Moment Gyros," *Journal of the Astronautical Sciences*, Vol. 46, No. 3, July–Sept. 1998, pp. 307–328.

[24] Schaub, H., and Junkins, L. J., "Singularity Avoidance Using Null Motion and Variable-Speed Control Moment Gyros," *Journal of Guidance, Control, and Dynamics*, Vol. 23, No. 1, Jan.–Feb. 2000, pp. 11–16. doi:10.2514/2.4514

[25] Richie, D. J., Lappas, V. J., and Prassinos, G., "A Practical Small Satellite Variable-Speed Control Moment Gyroscope for Combined Energy Storage and Attitude Control," *Acta Astronautica*, Vol. 65, Nos. 11–12, Dec. 2009, pp. 1745–1764. doi:10.1016/j.actaastro.2009.05.005

[26] Stevenson, D., and Schaub, H., "Nonlinear Control Analysis of a Double-Gimbal Variable-Speed Control Moment Gyroscope," *Journal of Guidance, Control, and Dynamics*, Vol. 35, No. 3, May–June 2012, pp. 787–793.
doi:10.2514/1.56104

[27] Zhang, H., and Fang, J., "Robust Backstepping Control for Agile Satellite Using Double-Gimbal Variable-Speed Control Moment Gyroscope," *Journal of Guidance, Control, and Dynamics*, Vol. 36, No. 5, Sept.–Oct. 2013, pp. 1356–1363.
doi:10.2514/1.59327

[28] Jikuya, I., Fujii, K., and Yamada, K., "Attitude Maneuver of Spacecraft with a Variable-Speed Double-Gimbal Control Moment Gyro," *Advances in Space Research*, Vol. 58, No. 7, Oct. 2016, pp. 1303–1317.
doi:10.1016/j.asr.2016.06.010

[29] Cui, P., and He, J., "Steering Law for Two Parallel Variable-Speed Double-Gimbal Control Moment Gyros," *Journal of Guidance, Control, and Dynamics*, Vol. 37, No. 1, Jan.–Feb. 2014, pp. 350–359.
doi:10.2514/1.60403

[30] Sasaki, T., and Shimomura, T., "Fault-Tolerant Architecture of Two Parallel Double-Gimbal Variable-Speed Control Moment Gyros," *AIAA Guidance, Navigation, and Control Conference, AIAA SciTech Forum*, AIAA Paper 2016-0090, 2016.
doi:10.2514/6.2016-0090

[31] Schaub, H., and Junkins, J. L., *Analytical Mechanics of Space Systems*, 3rd ed., AIAA Education Series, AIAA, Reston, VA, 2014, pp. 44, 45, 117–126.
doi:10.2514/4.102400

[32] Schaub, H., and Junkins, J. L., "Stereographic Orientation Parameters for Attitude Dynamics: A Generalization of the Rodrigues Parameters," *Journal of the Astronautical Sciences*, Vol. 44, No. 1, Jan.–March 1996, pp. 1–19.

[33] Tani, Y., and Okubo, H., "Singularity Robust Steering of Redundant Single Gimbal Control Moment Gyros for Small Satellites," *Proceedings of i-SAIRAS 2005, the 8th International Symposium on Artificial Intelligence, Robotics and Automation in Space*, Munich, Germany, Sept. 2005, pp. 603–609.

[34] Sidi, M., *Spacecraft Dynamics and Control, A Practical Engineering Approach*, Cambridge Univ. Press, New York, 1997, pp. 241–242.
doi:10.1017/CBO9780511815652

E. G. Lightsey
Associate Editor